Journal of Materials Chemistry A

Accepted Manuscript

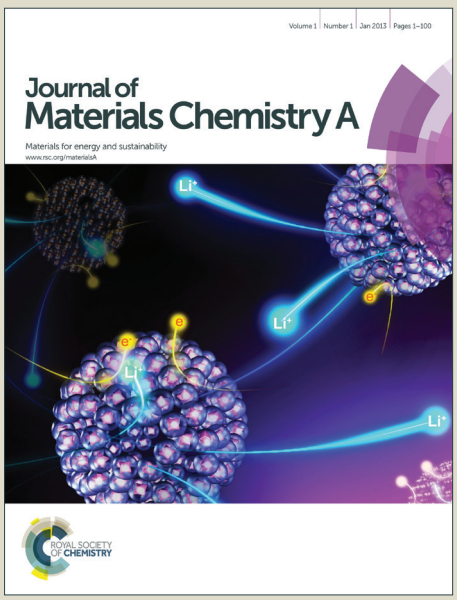

ROYAL SOCIETY OF CHEMISTRY

www.rsc.org/materialsA

Journal Name

RSCPublishing

ARTICLE

Sulfur double locked by macro-structural cathode and solid polymer electrolyte for lithium-sulfur battery

Cite this: DOI: 10.1039/x0xx00000x

Received 00th January 2012,
Accepted 00th January 2012

DOI: 10.1039/x0xx00000x

www.rsc.org/

Cheng Zhang,[a] Yue Lin [a] and Jin Liu [*a,b]

Both macro-structural cathode materials and metal-organic framework (MIL-53(Al)) modified solid polymer electrolyte are used to inhibit polysulfide dissolution and shuttling in all-solid-state lithium-sulfur battery. At 80 °C, the discharge capacities of 1520 mAh g^{-1} in the first cycle at 0.2 C, and 325 mAh g^{-1} in the 1000th cycle at 4 C are obtained, demonstrating exceptional high-rate capability and long-term cycling performance of the batteries. Mechanisms for such enhancement are investigated by cyclic voltammetry, X-ray photoelectron spectroscopy (XPS), electrochemical impedance spectroscopy (EIS), and thermo-gravimetric analysis techniques. In the EIS spectra there is no semicircle caused by the polysulfide shuttling and reacting at the electrolyte/Li interface, proving that polysulfide dissolution is adequately inhibited. In the XPS spectra, no peak of sulfur and polysulfide is found on the Li anode surface after 10 discharge/charge cycles, showing that sulfur and polysulfide do not transfer from the cathode to the anode. The -C-S- bond in the original cathode is observed by XPS, indicating that sulfur is linked on macro-structural cathode materials by the thermal treatment. In addition, an intermediate forms during cycling and displays steady electrochemical reversibility. These data indicate that the macro-structural cathode and solid polymer electrolyte play crucial roles in blocking polysulfide dissolution and shuttling, and lead to the outstanding cycling performance of all-solid-state lithium-sulfur battery.

Introduction

In lieu of demands for high-density and lightweight energy storage, lithium-sulfur battery holds promise as a sustainable method to address accelerating rates of the energy requirements. Compared to state-of-the-art lithium-ion batteries, lithium-sulfur battery has higher theoretical capacity of 1672 mAh g^{-1} that is receiving increasing attention.[1-6] Meanwhile, the abundance and environmental friendliness of sulfur also make lithium-sulfur battery appealing.[7] However, utilization of active materials is low due to polysulfide dissolution and shuttling as well as poor electronic conductivity of elemental sulfur, and as a result, deteriorate the performance of lithium-sulfur battery.[8-16]

In order to improve the performance of lithium-sulfur batteries, various methods have been employed including modification of active materials structure, optimization of separator and components of organic liquid electrolyte.[13-15] However, in traditional liquid lithium–sulfur cells, the polysulfide shuttle and lithium dendrite formation are still unavoidable. Thus, employing solid electrolytes instead of liquid electrolytes is an optimal choice in terms of eliminating the polysulfide shuttle and protecting metallic lithium anodes, which benefits to enhance the cycling performance, stability and safety of lithium–sulfur batteries.[13,17] Especially, all-solid-state lithium-sulfur battery based on solid polymer electrolyte (SPE) possesses not only high capacity but also great flexibility, which makes designs and manufactures available for fashionable energy storage devices and electric vehicles. [18-21] Previous studies showed the all-solid-state lithium-sulfur battery using ZrO_2 modified solid polyethylene oxide (PEO) electrolyte delivered the discharge capacity of 900 mAh g^{-1} at a 0.05 C rate and 90 °C.[19] Recently, the battery using solid polymer electrolyte (PEO_{18}-$Li(CF_3SO_2)_2N$+10wt% SiO_2) presented the discharge capacity of 800 mAh g^{-1} after 25 cycles at a current density of 0.1 mA cm^{-2} and 70 °C.[20] However, all-solid-state lithium-sulfur battery with high capacity and long cycling performance has not been achieved.

In this study, we develop an efficient method to inhibit polysulfide dissolution and shuttling in all-solid-state lithium-sulfur battery by using metal-organic framework (MIL-53(Al)) modified SPE and macro-structural sulfur cathode. The electrolyte is a flexible thin film modified by porous metal-organic framework materials displaying higher ionic conductivity compared to the PEO electrolytes with nanoparticles.[19,20,22] The cathode materials were prepared by polymerization of aniline with the mixture of sublimed sulfur and conductive carbon at 0 °C, followed by thermal treatment at 280 °C. The all-solid-state lithium-sulfur battery consisting of the composite cathode, the solid polymer electrolyte and lithium anode

delivers the initial discharge capacity of 1520 mAh g^{-1} at 80 °C and 0.2 C. At a higher rate of 4 C at 80 °C, this kind of battery displays a long cycling with the discharge capacity of 325 mAh g^{-1} in the 1000th cycle. Both capacity and cycling performance are significantly enhanced compared to the previous reports.[18-20]

Mechanisms for such enhancement of battery performance were investigated by using cyclic voltammetry (CV), X-ray photoelectron spectroscopy (XPS), electrochemical impedance spectroscopy (EIS), and thermo-gravimetric (TG) analysis techniques. In the first CV cycle, it is found that there are two reduction peaks at 2.38 V and 2.03 V and one oxidation peak at 2.29 V. In the following CV cycles, the reduction peak at 2.38 V disappears, while another reduction peak shifts to higher potential of 2.10 V and the position of the oxidation peak does not change, indicating an irreversible reduction reaction occurred at 2.38 V that results in the first irreversible capacity fade. The relative discharge/charge curves present similar results that two indistinguishable discharge plateaus are merged into one reversible curve after the first discharge/charge cycle, revealing this reduction reaction in the peak position of 2.10 V is reversible. In the EIS spectra there is no semicircle caused by the polysulfide shuttling and reacting at the electrolyte/Li interface, proving that polysulfide dissolution is adequately inhibited. In addition, the -C-S- component is observed in the original cathode materials by XPS and it is still present in the XPS spectra of the cathode after discharge/charge cycles, directing that sulfur is stably linked on macro-polyaniline (PANI) by the thermal treatment. These data indicate that macro-structural cathode materials and the solid polymer electrolyte play crucial roles on blocks of polysulfide dissolution and shuttling, which contribute to the outstanding performance of the all-solid-state lithium-sulfur battery.

Experimental section

Materials

Aniline (C_6H_7N, +99.5%), ammonium persulphate ($[NH_4]_2S_2O_8$, 98.5%), sublimed sulfur (S, 99.95%), super P, hydrochloric acid (HCl, AR grade), polyethylene oxide (PEO, M_w=4000000, 99.9%), and acetonitrile (CH_3CN, AR grade), were obtained from Aladdin. Lithium bis(trifluoro-methanesulfonyl)imide (LiTFSI, +99.5%) was purchased from Sigma Aldrich and stored in a glove box. N-methyl-2-pyrrolidone (NMP, 99.5%) was purchased from Heowns.

Preparation of PANI@C/S-280

0.1000 g conductive carbon black (Super P) and 0.7000 g sublimed sulfur were milled for 1 h to obtain C/S composite. The composite was dispersed in 100 mL deionized water and sonicated for an hour to form uniform suspension. 0.2 mL aniline and 20 mL hydrochloric acid (2 M) were added into the suspension and stirred for 1 h. Subsequently, 0.6500 g ammonium persulphate in 30 mL deionized water was added dropwise to the above mixture, and it was cured at 0 °C for 12 h to in-situ perform polymerization of aniline. The obtained precipitate was filtered and washed for 3 times with distilled water, and then dried in a vacuum oven at 50 °C for 24 h. Dark green powder of polymerized PANI/C/S composite was obtained. The powder was sealed into a glass tube filled with argon and heated to 280 °C and kept 280 °C for 12 h to gain the modified PANI/C/S composite labelled as PANI@C/S-280.

Preparation of solid polymer electrolyte membrane

Preparation of solid polymer electrolyte thin film was carried out according to our previous report.[22] PEO was thoroughly dried at 50 °C for 12 h, and LiTFSI was dried at 100 °C in a vacuum for 24 h before use. Firstly, 0.1300 g LiTFSI was added to 8 mL acetonitrile and stirred for 1 h. Then, 0.0300 g MIL-53(Al) nano-particles and 0.3000 g PEO were added to the solution respectively and stirred for 36 h. A homogenized colloidal solution of PEO-LiTFSI-MIL-53(Al)-CH_3CN was formed. The solution was cast on plastic sheeting and dried at 80 °C for 24 h in an argon-filled gloved box to remove the solvent acetonitrile. Finally, a PEO-MIL-53(Al)-LiTFSI thin film electrolyte was formed and the thickness of the solid electrolyte thin film is about 60 μm.

Electrochemical measurements

All-solid-state lithium-sulfur battery was assembled by contacting in sequence a lithium metal disk anode, a layer of the electrolyte membrane, and a disk cathode. The cathode was fabricated from slurry of PANI@C/S-280, carbon black (Super P) and binder (80:10:10 by weight). The slurry was then coated onto aluminium foil using a doctor blade and dried at 50 °C to form a working electrode. Galvanostatic discharge/charge tests were performed in the potential range of 1.0-3.0 V (versus Li^+/Li) at 80 °C by using a LAND battery-testing instrument (Wuhan Land Electronic Co., Ltd. China). Cyclic voltammetry (CV) and electrochemical impedance spectroscopy (EIS) measurements were conducted using a PARSTAT 4000 electrochemical measurement system. CV tests were performed at a scan rate of 0.2 mV s^{-1} in the voltage range of 1.0-3.0 V. EIS measurements were carried out at open-circuit potential (OCP) in the frequency range between 100 kHz and 100 mHz with a perturbation amplitude of 5 mV. All measurements, such as the test of the discharge/charge cycling, CV and EIS were performed under temperature controlled ovens with a standard deviation of 1 °C.

Materials characterization

Thermal behaviour of samples was investigated by thermo gravimetric analysis (TGA, SDTQ600) under an Ar atmosphere at a heating rate of 10 °C min^{-1} from 20 °C to 800 °C. An elemental analyzer (Vario MICRO) was applied to determine the components of the composite (average value from more than 10 regions). The S content in PANI@C/S-280 determined was 43.0% that was used to calculate the battery capacity. And the areal loading amount of the sulfur is about 0.8 mg cm^{-2} according to the sulfur content of PANI@C/S-280 and the area of disk cathode. The morphology of the sample was investigated by transmission electron microscopy (TEM, Tecnai G2 20ST) and the elements on the surface of sample were identified by scanning transmission electron microscopy (STEM, Tecnai G2 F20). XPS measurement was performed using a SPECS system, an ultrahigh vacuum (UHV) system (< 2×10^{-10} mbar) equipped with a monochromatic Al Ka (1486.7 eV) X-ray in situ. Al Ka radiation was operated at 100 W and the pass energy of the spectrometer with a resolution of 0.5 eV was 40 eV. The binding energy was all referenced to the Fermi level position of the electron analyzer. The XPS of the cathode/electrolyte interface before cycles (labelled as "Original") and after 1st (labelled as "After 1st cycle"), 2nd (labelled as "After 2nd cycle") cycles were obtained. The XPS spectrum of PANI@C/S-280 based cathodes (Original) before cycling was tested without assembling into the battery. The XPS spectra of the cathode/electrolyte interface after 1st or 2nd cycling were obtained by removing the electrolyte membrane and lithium anode from the batteries that ran 1 or 2 discharge/charge cycles at 80 °C and 0.2 C.

Results and discussion

Microstructure, elemental components and thermal stability of PANI@C/S-280 cathode materials and cycling performance of the cathode/solid polymer electrolyte/Li battery

Fig. 1 shows the TEM images and elemental mapping of the PANI@C/S-280 cathode materials. As shown in Fig. 1a, the materials appear as a stack of small spheres in a less than 100 nm scale. To recognize the elemental distribution, a square area in the red frame of Fig. 1b was chosen and tested. It is found in Fig. 1c and d that carbon and nitrogen are homogeneously distributed in the sample. Sulfur has a similar distribution as carbon and nitrogen, but its concentration changes in the regions of Fig. 1e.

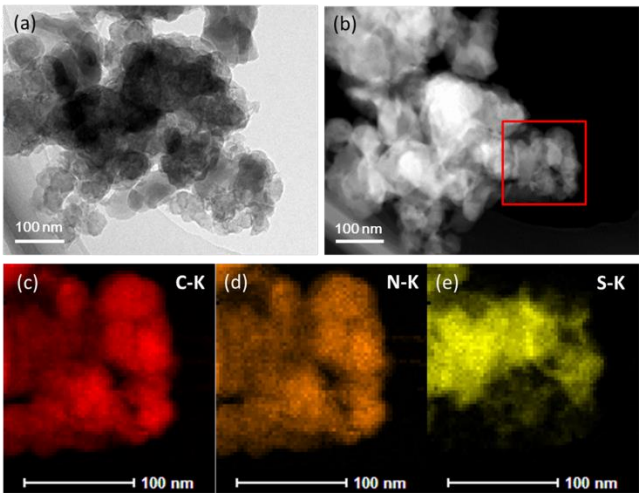

Fig. 1 (a) TEM image of PANI@C/S-280, (b) HAADF-STEM image of PANI@C/S-280 and corresponding elemental mapping across the selected area in the red frame of (c) carbon, (d) nitrogen, (e) sulfur.

Sulfur distribution can be affected by the ratio of conductive carbon to PANI. According to the elemental analysis, in which the S, C, H and N contents are separately 43.0 wt%, 51.6 wt%, 0.8 wt% and 5.3 wt%, nitrogen only comes from PANI molecules, while carbon comes from both PANI and conductive carbon. Although the distribution of carbon and nitrogen is homogeneous, conductive carbon may not be uniformly dispensed since there is a small portion of about 10 wt% conductive carbon in the materials as prepared. Besides, conductive carbon hardly captures sulfur through undertaking the 280 °C treatment.[23] Hence, the concentration of sulfur in the shade part of Fig. 1e lowers as an increase of the conductive carbon/PANI ratio. As a corollary, sulfur is more likely to combine with PANI and evenly to allocate around PANI.

Thermo gravimetric analysis of PANI@C/S-280 materials and sublimed sulfur was carried out in an Ar atmosphere with a heating rate of 10 °C min^{-1} from 20 to 800 °C, as shown in Fig. 2. The sublimed sulfur (cyclic-S_8) loses weight from 200 °C to 320 °C. For the PANI@C/S-280 materials, no obvious weight loss below 405 °C is observed. Until 800 °C, about 51.5% weight remains that is chiefly ascribed to PANI-sulfides and conductive carbon. This increase up to 205 °C in the first weight loss temperature illustrates that the PANI@C/S-280 materials are more thermally stable compared to elemental sulfur. This result also reveals that elemental sulfur is not essentially present in the PANI@C/S-280 materials after the treatment at 280 °C for 12 hours.

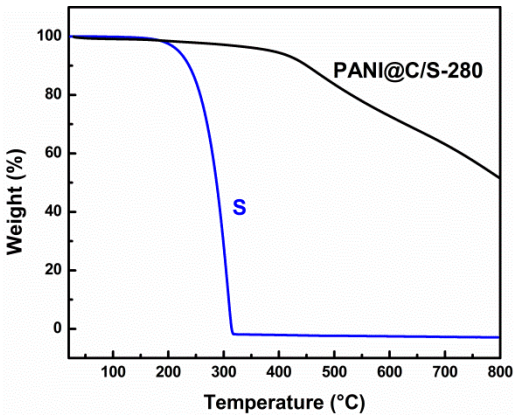

Fig. 2 Thermogravimetric curves of sublimed sulfur and PANI@C/S-280 materials measured from 20 to 800 °C in an Ar atmosphere with a heating rate of 10 °C min^{-1}.

Previous studies found that polysulfide dissolution and shuttling caused fast decay of battery capacities.[4,6,12] In order to examine the effect, the cycling performance of all-solid-state lithium-sulfur batteries fabricated with the PANI@C/S-280 materials as cathode, the solid polymer electrolyte membrane as electrolyte, and pure lithium metal as anode was carried out. Each battery was discharged first and then charged as a full cycle. Fig. 3a is the result of the battery cycled at 80 °C and 0.2 C. The initial discharge capacity is 1520 mAh g^{-1}, the initial charge capacity is 920 mAh g^{-1}, and the second discharge capacity is 906 mAh g^{-1}. After undergoing 60 discharge/charge cycles, the battery still maintains the discharge capacity of 876 mAh g^{-1}, with capacity retention of 96.7% based upon calculation on the second discharge capacity.

To acquire insight into kinetics evolution of interface impedance during discharge/charge cycles of the battery, EIS was performed. Fig. 3b is the EIS spectra of the battery in the original state (undischarged and uncharged) and after the 1st, 2nd, 3rd and 30th cycles at 80 °C and 0.2 C. The EIS spectra consist of a semi-circle at the high frequency region, whose diameter gives the charge-transfer resistance R_{ct}, and an inclined line in the low frequency region, which corresponds to the mass-transfer process.[24,25] The high-frequency intercept on the real axis represents the ohmic resistance (R_o) of the cell, including the electrolyte and electrode resistances.[26,27] The data obtained from EIS are fitted by the equivalent circuit as shown in the inset of Fig. 3b. R_o are 23.2 Ω for the original battery, and 18.9, 19.2, 18.9 and 19.1 Ω respectively for the battery after the 1st, 2nd, 3rd and 30th cycles, testifying solid transferring ability of lithium ions in the bulk of solid electrolyte and electrodes. Besides, R_{ct} for the original battery is 33.7 Ω, and those are 34.1, 35.4, 35.2 and 33.8 Ω after the 1st, 2nd, 3rd and 30th cycles, respectively. The averaged R_{ct} of 34.4 Ω with a small standard deviation of ±0.8 Ω reveals a steady electrochemical environment in the battery. Moreover, no additional semicircle caused by the polysulfide shuttling and reacting at the electrolyte/Li interface is found.[28] These results demonstrate that polysulfide dissolution and shuttling are adequately inhibited by the combination of PANI@C/S-280 cathode and solid polymer electrolyte in the all-solid-state lithium-sulfur battery.

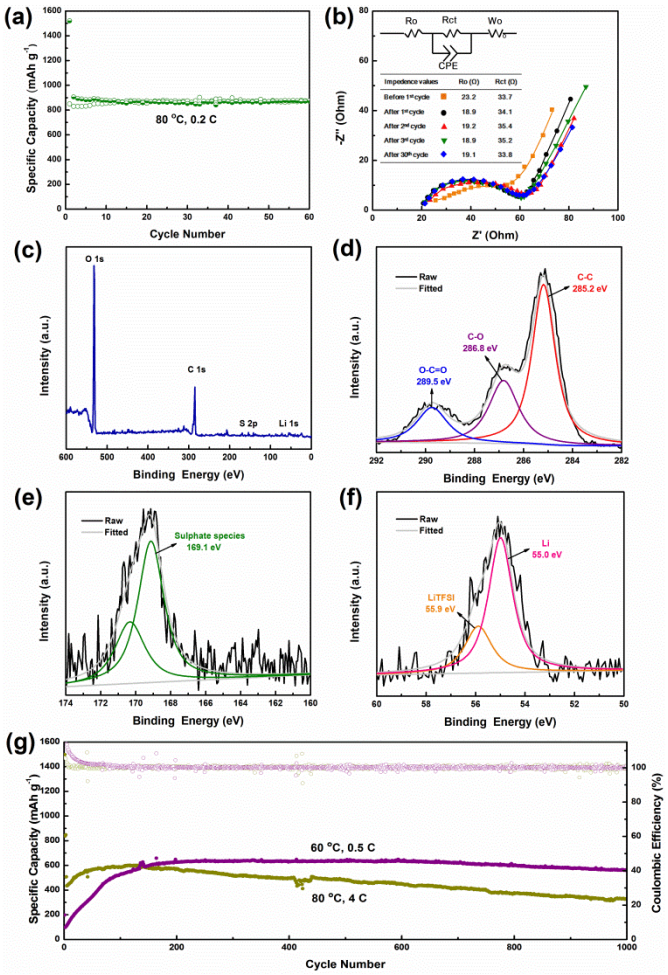

Fig. 3 (a) Discharge (half down circle) and charge (hollow circle) capacity of PANI@C/S-280 materials based all-solid-state lithium-sulfur battery at 80 °C, 0.2 C (1 C = 1672 mAh g^{-1}), (b) EIS spectra of PANI@C/S-280 cathode based all-solid-state lithium-sulfur battery after certain cycles at 80 °C, 0.2 C, scatter represents original data, line represents fitting results using the circuit inset. (c) Full-spectrum, (d) C 1s, (e) S 2p, and (f) Li 1s XPS spectra on the anode surface after cycling the tenth discharge/charge cycle of the battery in which the cathode and electrolyte were removed from the battery. (g) Discharge capacity (solid circle) and Coulombic efficiencies (open circle) of the batteries at 80 °C, 4 C (dark yellow, after a three-cycle activation at 80 °C, 0.2 C) and at 60 °C, 0.5 C (purple).

For the sake of determining whether sulfur transport from the cathode to the anode**,** XPS was employed to detect the anode surface after the battery ran 10 discharge/charge cycles. The binding energy scale was corrected based on the C 1s peak around 284.8 eV as the internal standard, and the Shirley background, the mixed Gaussian/Lorentzian approach, is used to fit the C 1s ,S 2p and Li 1s peaks by the XPS peak software.

From the full-spectrum in Fig. 3c, there are two obvious peaks belonging to the O 1s and C 1s that are mainly derived from the electrolyte. As shown in Fig. 3d, three states of carbon including C-C, C-O and O-C=O bonds are present, which are attributed to PEO, LiTFSI and MIL-53(Al) of the electrolyte.[29,30] In addition, the peak of Li 1s is weak in the full-spectrum due to relatively low sensitivity of Li itself and partial overlapping by the electrolyte. However, the weak S 2p signal is probably attributed to a low proportion in the sample. As shown in Fig. 3e, one peak located at 169.1 eV appears, which is corresponding to sulfur species of LiTFSI.[31] Two states of lithium ascribing to LiTFSI (55.9 eV) and Li metal (55.0 eV) are observed in Fig. 3f, which are agreement with the previous report.[32] There are no S (164.0 eV), Li_2S_n ($2<n<8$) (162.0 eV~164.0 eV) and Li_2S_2/ Li_2S (~161.0 eV)[32,33] in the Li anode, demonstrating no sulfur or polysulfide transport from the cathode to the anode.

Previous studies found that amounts of nitrogen in the PANI cathode materials can inhibit polysulfide dissolution through chemical adsorption of the amine groups.[34-38] Besides, surfaces of MIL-53(Al) nano-particles showed strong Lewis acid properties, which can adsorb abundant anionic groups (TFSI-) of lithium salt. So, the MIL-53(Al)-TFSI- as an integral has electronegativity to reject polysulfide anions by the electrostatic interaction and further effectively restrains polysulfide dissolution.[22] Consequently, sulfur is double locked by the macro-structural cathode and solid polymer electrolyte.

A fast discharge/charge ability of the high-capacity all-solid-state lithium-sulfur battery was also investigated. Fig. 3g presents the higher rate cycling performance of the battery. At 80 °C and 4 C, the discharge capacity is 507 mAh g^{-1}. This capacity is obtained after a three-cycle activation process at a low rate of 0.2 C at 80 °C. Undertaking about a 100-cycle activation process, the highest discharge capacity reached is 601 mAh g^{-1}, which is due to the serious electrochemical polarization and an incomplete utilization of the active materials at the high rate. As cycles continue, more lithium ions move at the electrode interface and infiltrate into the interior of the cathode. Eventually, inactive sulfur on the internal surfaces is able to be reutilized and stable capacities are present in the subsequent cycles.[10,11,39] Even over 1000 cycles, a stable discharge capacity of 325 mAh g^{-1} with an average capacity loss of 0.31 mAh g^{-1} per cycle is attained.

For further testing battery cycling performance, a battery was cycled at 60 °C and 0.5 C and the result is present in Fig. 3g as well. After ~200 cycles, the maximum discharge capacity of 640 mAh g^{-1} is gained. Over 1000 discharge/charge cycles, a reversible discharge capacity of 558 mAh g^{-1} remains, attaining 87% capacity retention. Thus, both capacity and cycling performance are dramatically improved by the integrated method.

It is noticed that there is a long activation process for reaching the maximum capacity of batteries. This is mainly due to the inferior ionic conductivity of the solid polymer electrolyte. The slow migration of Li^+ ions into electrode surfaces may lead to incomplete electrochemical reaction. In addition, weak compatibility between solid electrolyte and solid electrodes interfaces may cause the extension of the activation cycles. However, this process can be shortened by activating batteries at higher temperatures.

Effects of structures at the cathode/electrolyte interface on battery performance

Fig. 4a exhibits the discharge/charge profiles of the PANI@C/S-280 cathode based lithium-sulfur battery at 80 °C and 0.2 C that corresponds to the data shown in Fig. 3a. In the first discharge cycle, two distinguishable plateaus at 2.5-2.3 V and 2.2-1.8 V are seen. The total initial discharge capacity is 1520 mAh g^{-1}, and the discharge capacity between 2.5 and 2.3 V is about 251 mAh g^{-1}. During the first charging process, only one plateau at 2.1-2.3 V is present, and the initial charge capacity is 920 mAh g^{-1}. In the second discharge cycle, the plateau at 2.5-2.3 V disappears and alternatively a long and sloped curve at 2.2-1.8 V appears with a capacity of 910 mAh g^{-1}. The capacity holds in the following discharge and charge cycles. Additionally, the second discharge/charge curves overlap in the third

curves, illuminating that the discharge and charge processes are reversible after the first cycle.

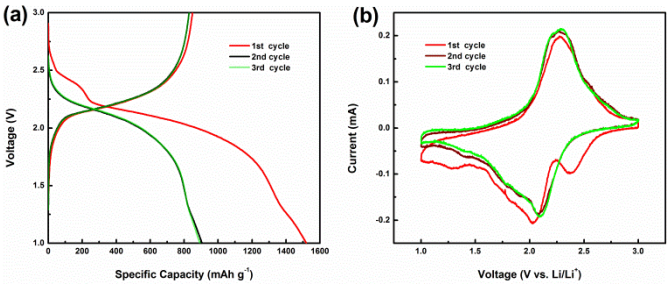

Fig. 4 (a) Discharge/charge curves of the all-solid-state lithium-sulfur battery at 80 °C and 0.2 C. (b) Cyclic voltammograms of the all-solid-state lithium-sulfur battery in the voltage of 3.0-1.0 V at 80 °C and a scan rate of 0.1 mV s^{-1}.

CV curves of the battery are present in Fig. 4b. In the first cathodic scan, there are two remarkable reduction peaks at 2.03 V and 2.38 V, but in the first anodic scan, only one oxidation peak at approximately 2.29 V is observed. In the second and third cycles, the position of the oxidation peak does not change, while the reduction peak at 2.38 V disappears and the reduction peak at 2.03 V moves to a little bit higher position of 2.10 V, revealing a reduced polarization after the first cycle.[40,41] In addition, the CV curves of the second and third cycles are basically met, which is in agreement with the discharge/charge characteristics in Fig. 4a.

It is noted that the cycling behavior is quite different from that of traditional lithium-sulfur batteries reported.[42-44] For a typical lithium-sulfur battery using organic liquid electrolyte, the discharge curves generally show an obvious two-plateau behavior.[45,46] The first plateau at 2.5-2.3 V associated with the conversion of the active materials from cyclic-S_8 to soluble lithium polysulfide (Li_2S_n, $4<n\leq8$) finally to soluble Li_2S_4, and the second plateau was the reduction of Li_2S_4 to Li_2S_2 finally to Li_2S.[47-49] During the charging process, Li_2S was delithiated to form Li_2S_4 and eventually S_8.[50,51] In the initial discharge cycle of Fig. 4a, the first plateau may associate with high polymerized sulfur reduced to S_4^{2-}, and the second plateau is related to the S_4^{2-} transferred into S^{2-}. In the following discharge process, but, the two plateaus occurred in the first discharge process are merged into a long sloping curve. This suggests that there is an intermediate different from the S_4^{2-} state after the first discharge/charge cycle.

XPS experiments were carried out to understand the intermediate structure. Fig. 5 shows the S 2p and C 1s XPS spectra of the cathode/electrolyte interface before cycling, after the first discharge/charge and the second discharge/charge cycles.

For the S 2p spectra, two doublets are used to fit the peaks, and each doublet is made up of S $2p_{3/2}$ and S $2p_{1/2}$. Compared to the typical binding energy values, the peaks located at 163.7 eV and 164.9 eV in the S 2p spectrum (Original) represent -C-S- bonds.[52] Concurrently, the C 1s spectrum (Original) also exhibits a signal of -C-S- at the binding energy of 285.4 eV, proving again the existence of -C-S- bonds in the original cathode.[30,53] Besides, the peaks at 164.0 eV and 165.2 eV in the S 2p spectrum of the original cathode are assigned to the -S-S- bonds,[32,54] which are mainly from sulfur linking to PANI during the high temperature process.

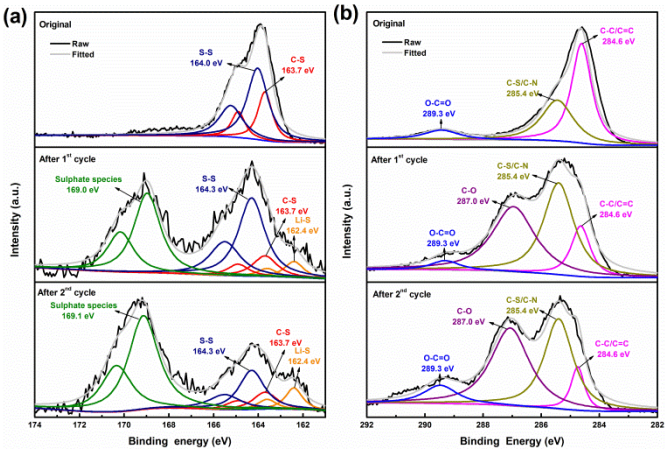

Fig. 5 (a) S 2p and (b) C 1s XPS spectra of the cathode/electrolyte interface before cycling (labeled as Original), after the first discharge/charge cycle (labeled as After 1st cycle) and after the second discharge/charge cycle (labeled as After 2nd cycle).

S 2p spectrum of the cathode/electrolyte interface after first cycle presents four kinds of sulfur. The broad peak at around 169.0 eV is a result of sulfate species coming from the solid electrolyte. The peaks at 164.3 eV and 165.5 eV are assigned to -S-S- bonds. The peaks at 163.7 eV and 164.9 eV represent -C-S- bond. The peak at 162.4 eV could come from Li-S- in the intermediate, which is either a macro-structure of Li-S_n-C- bound to PANI or a micro form of Li-S_n-Li restrained by solid polymer electrolyte. Previous study found that the binding energy of sulfur in Li_2S_2 or Li_2S was in the range of 160.0-162.0 eV, and the binding energy of S_8 was about 164.0 eV.[32,33,55,56] Here, the value of n in Li-S_n-C- or Li-S_n-Li is inferred to be greater than 2. However, the specific structure of the intermediate needs to be further investigated.

Moreover, the signals of the four kinds of sulfur are also observed, and there are no other peaks in the S 2p spectrum of the cathode/electrolyte interface after the second cycle, validating that the intermediate is electrochemically reversible.

The other peak assignments in C 1s spectra in Fig. 5b are illustrated as follows. The peak at 289.4 eV is ascribed to -O-C=O groups from the binder.[30] The peak at 287.0 eV is from -C-O- bonds in PEO.[29] The peak at 284.6 eV is attributed to the -C=C- or -C-C- bonds mainly from PANI and conductive carbon.[31] The C 1s spectrum after the 2nd cycle has the same binding energy as that after the 1st cycle. These results further announce the intermediate has respectably electrochemical reversibility.

Conclusions

All-solid-state lithium-sulfur batteries were designed and prepared by the PANI@C/S-280 cathode, MIL-53(Al) metal-organic framework modified flexible solid electrolyte, and Li anode. The batteries exhibit outstanding electrochemical performance and cycling stability. At 80 °C and 0.2 C, the battery has a stable capacity of 876 mAh g^{-1}. After 1000 cycles at 80 °C, 4 C and 60 °C, 0.5 C, the discharge capacities of 325 mAh g^{-1} and 558 mAh g^{-1}, respectively can be obtained. These firmly demonstrate that the combination of PANI@C/S-280 cathode and solid polymer electrolyte is an effective method to block the polysulfide dissolution and shuttling and to enhance battery performance. In addition, an electrochemically reversible intermediate is found in the battery during cycling. Further experiments are being performed to clarify the intermediate structure.

Acknowledgements

The authors thank Professor Yongli Gao, Lu Lv and Haipeng Xie in the institute of super-microstructure and ultrafast process in advanced materials at the Central South University for helpful discussions in the XPS experiments, and the reviewers of this manuscript for their comments and suggestions. This work was supported by funds from the National Natural Science Foundation of China (Grant No. 51274239) and Central South University.

Notes and references

[a] School of Metallurgy and Environment, Central South University, Changsha City, 410083, China. E-mail: jinliu@csu.edu.cn

[b] Institute of Super-microstructure and Ultrafast Process in Advanced Materials, Central South University, Changsha City, 410083, China

1 Y. X. Yin, S. Xin, Y. G. Guo and L. J. Wan, *Angew. Chem. Int. Ed.*, 2013, **52**, 2-18.

2 H. Wang, Y. Yang, Y. Liang, J. T. Robinson, Y. Li, A. Jackson, Y. Cui and H. Dai, *Nano Lett.*, 2011, **11**, 2644–2647.

3 N. Jayaprakash, J. Shen, S. S. Moganty, A. Corona and L. A. Archer, *Angew. Chem. Int. Ed.*, 2011, **50**, 5904–5908.

4 G. Zhou, S. Pei, L. Li, D. W. Wang, S. Wang, K. Huang, L. C. Yin, F. Li and H. M. Cheng, *Adv. Mater.*, 2014, **26**, 625–631.

5 T. Xu, J. Song, M. L. Gordin, H. Sohn, Z. Yu, S. Chen and D. Wang, *ACS Appl. Mater. Interfaces*, 2013, **5**, 11355–11362.

6 J. Wang, L. Lu, M. Choucair, J. A. Stride, X. Xu, H. Liu and H. Liu, *J. Power Sources*, 2011, **196**, 7030–7034.

7 A. Manthiram, Y. Fu and Y. Su, *Acc. Chem. Res.*, 2013, **46**, 1125–1134.

8 Z. W. Seh, H. Wang, P. Hsu, Q. Zhang, W. Li, G. Zheng, H. Yao and Y. Cui, *Energy Environ. Sci*., 2014, **7**, 672–676.

9 S. H. Chung and A. Manthiram, *Adv. Funct. Mater*., 2014, **24**, 5299–5307.

10 L. Xiao, Y. Cao, J. Xiao, B. Schwenzer, M. H. Engelhard, L. V. Saraf, Z. Nie, G. J. Exarhos and J. Liu, *Adv. Mater*., 2012, **24**, 1176–1181.

11 G. Li, G. Li, S.Ye and X. Gao, *Adv. Energy Mater*., 2012, **2**, 1238–1245.

12 S. S. Zhang, *J. Power Sources*, 2013, **231**, 153–162.

13 A. Manthiram, Y. Fu, S. H. Chung, C. Zu and Y. S. Su, *Chem. Rev.*, 2014, **114**, 11751–11787.

14 Y. S. Su and A. Manthiram, *Nat. Commun.*, 2012, **3**, 1166–1172.

15 M. Q. Zhao, Q. Zhang, J. Q. Huang, G. L. Tian, J. Q. Nie, H. J. Peng and F. Wei, *Nat. Commun.*, 2014, **5**, 3410–3418.

16 Z. Lin, Z. Liu, W. Fu, N. J. Dudney and C. Liang, *Angew. Chem. Int. Ed.*, 2013, **52**, 7460–7463.

17 Z. Lin and C. Liang, *J. Mater. Chem. A*, 2015, **3**, 936–958.

18 S. S. Jeong, Y. T. Lim, Y. J. Choi, G. B. Cho, K. W. Kim, H. J. Ahn and K. K. Cho, *J. Power Sources*, 2007, **174,** 745–750.

19 J. Hassoun and B. Scrosati, *Adv. Mater.*, 2010, **22**, 5198–5201.

20 X. Liang, Z. Wen, Y. Liu, H. Zhang, L. Huang and J. Jin, *J. Power Sources*, 2011, **196**, 3655–3658.

21 G. Zhou, F. Li and H. –M. Cheng, *Energy Environ. Sci.*,2014, **7**, 1307–1338.

22 K. Zhu, Y. Liu and J. Liu, *RSC Adv.*, 2014, **4**, 42278–42284.

23 M. Rao, X. Y. Song and E. J. Cairns, *J. Power Sources*, 2012, **205**, 474–478.

24 X. Gao, J. Li, D. Guan and C. Yuan, *ACS Appl. Mater. Interfaces*, 2014, **6**, 4154–4159.

25 Z. Zhang, Q. Li, Y. Lai and J. Li, *J. Phys. Chem. C*, 2014, **118**, 13369–13377.

26 J. Q. Huang, Q. Zhang, H. J. Peng, X.Y. Liu, W. Z. Qian and F. Wei, *Energy Environ. Sci.*, 2014, **7**, 347–354.

27 Q. Tang, Z. Shan, L. Wang, X. Qin, K. Zhu, J. Tian and X. Liu, *J. Power Sources*, 2014, **246**, 253–259.

28 F. Wu, J. Z. Chen, L. Li, T. Zhao and R. J. Chen, *J. Phys. Chem. C*, 2011, **115**, 24411–24417.

29 C. Zhang, W. Lv, W. Zhang, X. Zheng, M. Wu, W. Wei, Y. Tao, Z. Li and Q. Yang, *Adv. Energy Mater.*, 2014, **4**, 1301565.

30 Z. Wang, Y. Dong, H. Li, Z. Zhao, H. Bin Wu, C. Hao, S. Liu, J. Qiu and X. W. Lou, *Nat. Commun.*, 2014, **5**, 5002–5010.

31 G. Zhou, L. Yin, D. Wang, L. Li, S. Peng, I. R. Gentle, F. Li and H. Cheng, *ACS Nano.*, 2013, **7**, 5367–5375.

32 Y. Diao, K. Xie, S. Xiong and X. Hong, *J. Electrochem. Soc.*, 2012, **159**, A1816–A1821.

33 Y. Z. Fu, C. X. Zu and A. Manthiram, *J. Am. Chem. Soc.*, 2013, **135**, 18044–18047

34 J. Song, M. L. Gordin, T. Xu, S. Chen, Z. Yu, H. Sohn, J. Lu, Y. Ren, Y. Duan and D. Wang, *Angew. Chem. Int. Ed.*, 2015, **54**, 1–6.

35 C. Tang, Q. Zhang, M. –Q. Zhao, J. –Q. Huang, X. –B. Cheng, G. –L. Tian, H. -J. Peng, and F. Wei, *Adv. Mater.*, 2014, **26**, 6100–6105.

36 C. Wang, K. Su, W. Wan, H. Guo, H. Zhou, J. Chen, X. Zhang and Y. Huang, *J. Mater. Chem. A*, 2014, **2**, 5018-5023.

37 X. Li, X. Li, M. N. Banis, B. Wang, A. Lushington, X. Cui, R. Li, T. –K. Sham and X. Sun, *J. Mater. Chem. A*, 2014, **2**, 12866–12872.

38 Y. Qu, Z. Zhang, X. Zhang, G. Ren, Y. Lai, Y. Liu and J. Li, *Carbon*, 2015, **84**, 399–408.

39 Y. –S. Su, Y. Fu and A. Manthiram, *Phys. Chem. Chem. Phys.*, 2012, **14**, 14495–14499.

40 R. Chen, T. Zhao, J. Lu, F. Wu, L. Li, J. Chen, G. Tan, Y. Ye and K. Amine, *Nano Lett.*, 2013, **13**, 4642–4649.

41 W. G. Wang, X. Wang, L. Y. Tian, Y. L. Wang and S. H. Ye, *J. Mater. Chem. A*, 2014, **2**, 4316-4323.

42 J. Zhou, R. Li, X. Fan,Y. Chen, R. Han,W. Li, J. Zheng, B. Wang and X. Li, *Energy Environ. Sci.*, 2014, **7**, 2715–2724.

43 D. W. Wang, Q. Zeng, G. Zhou, L. Yin, F. Li, H. M. Cheng, I. R. Gentle and G. Q. M. Lu, *J. Mater. Chem. A*, 2013, **3**, 9382–9394.

44 W. Weng, V. G. Pol and K. Amine, *Adv. Mater.*, 2013, **25**, 1608-1615.

45 L. Ji, M. Rao, H. Zheng, L. Zhang, Y. Li, W. Duan, J. Guo, E. J. Cairns and Y. Zhang, *J. Am. Chem. Soc*., 2011, **133**, 18522–18525.

46 L. Wang, Y. Zhao, M. L. Thomas and H. R. Byon, A*dv. Funct. Mater*., 2014, **24**, 2248–2253.

47 Y. Fu, Y. S. Su and A. Manthiram, *Adv. Energy Mater.*, 2014, **4**, 1300655.

48 Y. Yang, G. Zheng and Y. Cui. *Chem. Soc. Rev.*, 2013, **42**, 3018–3032.

49 X. Li, X. Li, M. N . Banis, B. Wang, A. Lushington, X. Cui, R. Li, T. K. Sham and X. Sun, *J. Mater. Chem. A*, 2014, **2**, 12866–12872.

50 B. Wang, Y. Wen, D. Ye, H. Yu, B. Sun, G. Wang, D. H. Jurcakova and L. Wang, *Chem. Eur. J.*, 2014, **20**, 1–8.

51 X. Yang, L. Zhang, F. Zhang, Y. Huang and Y. Chen, *ACS Nano.*, 2014, **8**, 5208–5215.

52 L. Xiao, Y. Cao, J. Xiao, B. Schwenzer, M. H. Engelhard, L. V. Saraf, Z. Nie, G. J. Exarhos and J. Liu, *J. Mater. Chem. A*, 2013, **1**, 9517–9526.

53 T. Lin, Y. Tang, Y. Wang, H. Bi, Z. Liu, F. Huang, X. Xie and M. Jiang, *Energy Environ. Sci.*, 2013, **6**, 1283–1290.

54 Z. Li, L. Yuan, Z. Yi, Y. Sun, Y. Liu, Y. Jiang, Y. Shen, Y. Xin, Z. Zhang and Y. Huang, *Adv. Energy Mater.*, 2014, **4**, 1301473.

55 R. D. Cakan, M. Morcrette, Gangulibabu, A. Gu ́eguen, R. Dedryv`ere and J. M. Tarascon, *Energy Environ. Sci.*, 2013, **6**, 176–182.

56 H. S. Kim, T. S. Arthur, G. D. Allred, J. Zajicek, J. G. Newman, A. E. Rodnyansky, A. G. Oliver, W. C. Boggess and J. Muldoon, *Nat. Commun.*, 2011, **2**, 427–433.

Graphical Abstract

All-solid-state lithium/sulfur batteries deliver the stable capacities of 910 mAh g^{-1}, which relate to the reversible reduction/oxidation of intermediate at 2.10 V/2.29 V.